

Structural determination of a palladium single crystal using photoelectron and Auger-electron angular distributions

Emir Güler and Kamil Klier

Zettlemoyer Center for Surface Studies, Lehigh University, Bethlehem, Pennsylvania 18015

(Received 6 April 1992)

The angular distributions of Pd $3d_{5/2}$ ($E_k = 1151.5$ eV), Pd $3d_{3/2}$ ($E_k = 1146.3$ eV), and Pd $3p_{3/2}$ ($E_k = 954.5$ eV) photoelectrons and Pd M_5VV Auger electrons ($E_k = 327.5$ eV) were investigated for a single-crystal Pd(100) surface. We have observed pronounced anisotropies in both photoelectron and Auger-electron intensities as a function of the polar emission angle θ along the principal azimuthal directions $\langle 001 \rangle$ and $\langle 011 \rangle$. We find that the observed angular distributions can be explained by the forward scattering of the outgoing electron waves (regardless of whether they are photoelectrons or Auger electrons) by the atoms overlying the emitter. Direct structural information was obtained by using the kinetic-energy dependence of the angular distributions of photoelectrons and Auger electrons in that zeroth-order forward-focused peaks are independent of energy, whereas the first-order interference intensities shift with energy. Forward-scattering spectroscopy is a very powerful technique in determining the relaxation of surface atoms despite a lack of translational symmetry normal to the surface. We have shown that the Pd(100) surface does not relax within 1.0° . The experimentally observed angular distributions are consistent with a single-scattering model in which forward focusing dominates the photoelectron and Auger-electron angular distributions.

INTRODUCTION

Forward-scattering spectroscopy is a structure-sensitive technique that has been developed for the study of surfaces during the past several years.^{1,2} It is based on the realization that the angular distribution of x-ray photoelectrons and Auger electrons with energies of a couple of hundred electron volts and above exhibit pronounced anisotropies that are structural in origin. These angular anisotropies are observed as *enhanced* intensities along the internuclear axes which connect the emitter atom to its nearest- and next-nearest-neighboring scatterer atoms. This technique makes use of a strong forward-scattering mechanism which occurs when photoelectron (Auger-electron) waves emitted by near-surface atoms are re-focused in the forward direction (i.e., forward scattering) due to the attractive potential of the atoms overlying the emitter. Combined with the chemical specificity of the photoelectrons and Auger electrons, this technique is a powerful diagnostic of the local structural environment around a particular emitter atom. This technique has important applications in areas such as direct determination of orientation of adsorbates, structures of epitaxially grown thin films, interdiffusion at interfaces, and surface segregations as discussed in recent reviews of the field.^{1,2} Forward-scattering spectroscopy can also be used directly to study lattice relaxations of near-surface atoms. In principle, changes in bond length and direction can be observed as a shift in the experimentally observed forward-focusing angles in proportion to the extent of the relaxation. Currently, the majority of the data in the literature comes from low-energy electron diffraction (LEED), where multiple-scattering effects may cause serious limitations in the interpretation.³ Forward-scattering

results are direct and the structures deduced from them are independent of any model.

Initial theoretical efforts have concentrated on the single-scattering model, which was applied by Davis and Kaplan to bare Cu(100).⁴ Some of the subsequent applications included chemisorption geometry of $c(2 \times 2)$ oxygen on Cu(100),⁵ bare Cu(100),⁶ and epitaxial Cu on Ni(100) (Ref. 7) surfaces. The single-scattering model can be described as a superposition of the primary wave excited from a given site and those waves scattered only once by atoms at other sites. The effects of inelastic scattering on wave amplitudes during propagation and vibrational attenuation of interference effects were incorporated into the single-scattering scheme.⁸ The single-scattering model has been used successfully to explain angular anisotropies. More recently, it became clear that in epitaxial Ni/Cu on a Ni(100) system, due to multiple-scattering effects, enhancements in the forward direction cannot be sustained for steadily larger overlayer thicknesses.^{2,9} A consequence of these effects is that strong forward-scattering enhancement in photoelectron and Auger-electron intensities originates from the top few atomic layers at the surface, with deeper layers making a more isotropic contribution. As a result, more sophisticated theories have emerged to address multiple-scattering effects.¹⁰⁻¹⁴ In the multiple-scattering formalism, the usual scalar scattering factor is replaced by a square matrix whose dimension determines the level of approximation. Recently, final-state effects were added to the existing schemes by the inclusion of the angular momentum of the initial state and the operational dipole selection rules.^{15,16} This resulted in a more-refined description of the angular distribution intensities. In the present work, we describe a simple single-scattering scheme adequate to

account for the experimental data.

It has been known for some time that in the case of Auger-electron emissions at kinetic energies below 200 eV the angular distributions produce results inconsistent with the forward-scattering mechanism.^{4,17-20} In Ref. 17, dated back to 1972, it was shown that the angular distribution of copper 62-eV $M_{2,3}VV$ Auger electrons produces a minimum at 0° using Cu(100) where the forward-scattering mechanism predicts a maximum. Over the years other researchers have observed other Auger-electron angular distribution "dips" in other materials, mostly in a low-energy regime. One recent finding in Pt(111), using 65-eV Pt Auger transitions and I and Ag overlayers on Pt (111), and using 355-eV Ag Auger transitions, showed a similar dip.²¹ Based on this result, it was suggested that the source of the discrepancy was the failure of the forward-scattering formalism and the way previous experiments were performed. Instead, a "silhouette" model was proposed, which stated that enhanced inelastic scattering of electrons out of low index directions by an atomic charge density is responsible for the observed intensity minima. This initiated a controversy that remains to be resolved. Interestingly, these dips were not observed in all materials. Furthermore, in the materials where they were observed, some of the Auger transitions did not exhibit the dips in forward-scattering directions. Additionally, a recent experiment using isoenergetic photoelectrons demonstrated that the angular distribution of 65-eV photoelectrons displayed a maximum at the polar emission angle of 0° , which is consistent with the forward-focusing mechanism.²⁰ No intensity minima have been reported along the principal crystallographic directions using photoelectrons, at any kinetic energy. It is therefore important to investigate the angular distributions of core-level photoelectrons and the Auger electrons in many different materials in order to shed more light on the mechanism involved.

We studied angular distributions of palladium photoelectrons (1151.5, 1146.3, and 954.5 eV) and Auger electrons (327.5 eV) emitted from the Pd(100) surface. Our results are entirely consistent with the forward-focusing model. The angular distribution of Auger electrons does not show any intensity minima corresponding to the bond directions. We have identified anisotropy associated with the zeroth-order forward focusing from the energy dependence of the photoelectron and Auger-electron angular distributions. This allowed us to directly determine the surface structure of the Pd(100) single crystal along the $\langle 001 \rangle$ and $\langle 011 \rangle$ azimuthal directions. The observed anisotropies are consistent with a single-scattering theory. But the relative intensities may await an interpretation based on a more-refined multiple-scattering theory incorporating final-state effects.

EXPERIMENTAL TECHNIQUE

The experiments described in this paper were conducted using a SCIENTA ESCA-300 x-ray photoemission spectrometer (XPS). This instrument has many useful features that are vital in producing angular distributions of photoelectrons and Auger electrons with high accura-

cy. The superior performance of ESCA-300 is partly due to a rotating anode as an x-ray source which can generate a finely focused, very intense x-ray beam at 8 kW, typically at 10 000 rpm. The high x-ray intensity reduces data-acquisition time dramatically. This minimizes the possibility of altering the surface conditions during the experiment due to background impurities, even at pressures as low as 10^{-10} Torr. The x-ray beam is then monochromatized using a monochromator with seven double-focusing 3-in.-diam quartz crystals. As a result, ESCA-300 features the highest obtainable resolution of 0.27 eV from the Fermi edge analysis of the Pt valence band. High angular resolution (7 msr) is obtained in the spatially resolved mode by the insertion of an additional prelens to the electrostatic lens system. In the same spatial mode in which angle-resolved XPS experiments are performed, lateral spatial resolution of less than $30 \mu\text{m}$ can be achieved for objects within 1.5 mm from the lens axis. A fixed, 600-mm-diam hemispherical analyzer, combined with a multichannel plate multidetector system, contributes significantly to the sensitivity and resolution of the overall system.

In the angle-resolved XPS experiments, sample manipulation was done manually by varying the polar emission angle (θ) and the azimuthal emission angle (ϕ) independently. Data for each set of experiments were recorded in a single data file using a multilayer structure (see Fig. 1). Experiments were performed in such a way that multiple scans of different kinetic energies were stored for each angle before the angle was incremented. This allowed us to measure the angular distribution of photoelectrons and Auger electrons, with varying kinetic energies, under the same experimental and geometrical conditions. In addition, storage of the data in layered structure facilitated the analysis under identical conditions for each scan. This approach minimizes random errors, making accurate comparisons of the angular distributions with different energies possible.

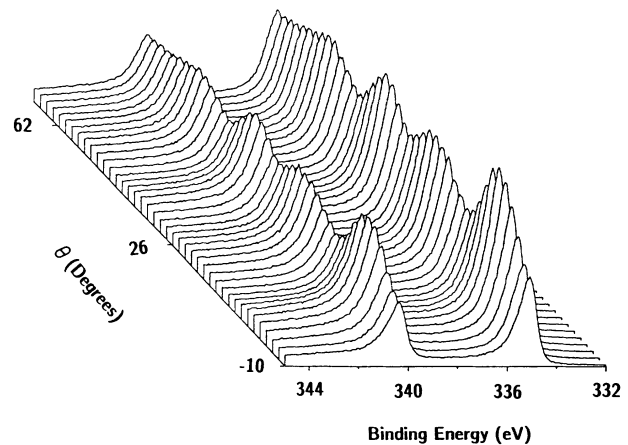


FIG. 1. A set of angle-resolved XPS data of the Pd $3d_{5/2}$ ($E_k = 1151.5$ eV) and Pd $3d_{3/2}$ ($E_k = 1146.3$ eV) recorded in the spatial mode along the $\langle 011 \rangle$ azimuth. The polar emission angle θ is scanned between -10° and 70° with 2° increments. Intensity variations in the angular distribution are clearly seen.

A high-purity Pd(100) single crystal was cleaned in two stages. Stage I was conducted in two bakeable ultrahigh-vacuum (UHV) systems. One consisted of a three-grid "display-type" low-energy-electron-diffraction (LEED) optics, an Auger-electron spectrometer (AES) with a cylindrical mirror analyzer, and a mass spectrometer (MS) for temperature-programmed desorption (TPD). The other system involved a high-resolution electron-energy-loss spectrometer (HREELS) and the MS. Each unit was evacuated by a 200-l/s ion pump boosted by a titanium sublimator. Typical background pressures were low, 10^{-10} Torr. Stage II was conducted in the preparation chamber of the ESCA-300.

The Pd(100) single crystal was spot welded between two 0.25-mm-diam Ta wires. This allowed rapid resistive heating of the crystals to 1000 K as measured by a chromel-alumel thermocouple spot welded to the crystal edge. Sulfur, carbon, nitrogen, and oxygen were encountered in the initial cleaning stages of the Pd(100) surface. Sulfur, nitrogen, and oxygen were readily removed by repetitive argon-ion etching and by heating the crystal to 1000 K. The removal of carbon was achieved by heating the crystal at 1000 K for 30 min in 5.0×10^{-8} Torr of oxygen. The oxygen was pumped out, the sample was allowed to cool to room temperature, and then the sample was ion etched to remove oxygen from the surface. After many of these cycles, further carbon removal was achieved by dosing the crystal with oxygen at room temperature and then flashing the crystal to 1000 K. This led to the desorption of CO and CO₂ as observed by TPD when carbon was present. This procedure was repeated until no background impurities were detected by AES, HREELS, TPD, and a sharp $p(1 \times 1)$ LEED pattern was observed.

After Stage-I cleaning, the sample was taken out of the UHV chamber and was oriented using Laue diffraction within $\pm 0.5^\circ$. Two small marks were scratched on the single crystal along the $\langle 001 \rangle$ direction. During the experiment these marks were used as a reference to align the analyzer axis with the desired direction by setting the azimuth angle. The polar emission angle (θ) was calibrated using a solid-state laser and the final alignment of the sample-holder-sample system was checked reflecting the laser beam into itself through a viewing port. The calibration of the azimuth angle was achieved by making accurate 45° and 90° marks on the sample-holder plate. Stage II of the cleaning procedure was conducted in the preparation chamber of the ESCA-300. A few cycles of argon sputtering and annealing around 1000 K, using backside electron bombardment heating, removed surface

oxide readily. Final cleanliness was checked by XPS and long-range order was verified by LEED. Experiments were performed using Al $K\alpha$ radiation ($h\nu = 1486.7$ eV) at room temperature.

RESULTS

Angular distributions of the various primary core-level emissions and an Auger transition were investigated using both single-crystal and polycrystal Pd. The core levels are Pd $3d_{5/2}$, Pd $3d_{3/2}$, and Pd $3p_{3/2}$ with emissions at kinetic energies of 1151.5, 1146.3 and 954.5 eV, respectively. The Pd M_5VV Auger transition at 327.5 eV was also studied in detail. A set of angle-resolved XPS data for the two Pd $3d$ emissions along the $\langle 011 \rangle$ direction, $\phi = 45^\circ$, is shown in Fig. 1. The x-ray beam spot size was estimated to be $30\mu \times 1.3$ mm. Here the data were recorded in the spatial mode between polar emission angles $\theta = -10^\circ$ and 70° with 2° increments. Anisotropy in the angular distribution of the photoelectrons is apparent. Figure 2 shows the angular distributions of the Pd $3d$ electrons, obtained from Fig. 1, along the $\langle 011 \rangle$ direction. Here, symbols represent experimental data points and the solid line is a cubic spline fit to the data. Both angular distributions are very similar, with four major peaks clearly identified at polar emission angles around 0° , 20° , 35° , and 54° . The observed anisotropy [$A = (I_{\max} - I_{\min}) / I_{\max}$] is $A = 45\%$ for Pd $3d_{5/2}$ and $A = 48\%$ for Pd $3d_{3/2}$ emissions. The full widths at half maximum (FWHM) of the angular distribution peaks of the two Pd $3d$ emissions are very similar and they are between 8.2° and 11.7° as shown in Table I. The degeneracy factor for the Pd $3d$ emissions was determined to be 1.42 ± 0.04 experimentally. This value is close to the expected value of $\frac{3}{2}$, i.e., $[(2J_1 + 1) / (2J_2 + 1)] = \frac{3}{2}$ for $J_1 = \frac{5}{2}$ and $J_2 = \frac{3}{2}$.

Similar experiments were also performed along the $\langle 001 \rangle$ direction, $\phi = 0^\circ$, using the same core-level photoelectrons. Figure 3 shows the angular distributions of the Pd $3d$ electrons as observed along the $\langle 001 \rangle$ direction. In this case four distinct peaks were identified at polar emission angles around 0° , 20° , 46° , and 70° . In this case the observed anisotropies were 38.2% and 40.9% for the Pd $3d_{5/2}$ and Pd $3d_{3/2}$ core levels, respectively. The angular distribution of the Pd $3d_{5/2}$ and Pd $3d_{3/2}$ core levels was also very similar along the $\langle 001 \rangle$ direction, with FWHM between 7.9° and 11.3° as shown in Table II. The degeneracy factor for the Pd $3d$ emissions along the $\langle 001 \rangle$ direction was 1.42 ± 0.06 .

TABLE I. Forward-scattering peak positions and FWHM of the Pd $3d$ core-level photoelectron angular distributions along the $\langle 011 \rangle$, $\phi = 45^\circ$ direction using the Pd(100) surface. Peak positions are determined by using a cubic spline fit to the data. Error bars on the data include only the uncertainty of locating the peak maximum.

Transition	Position	FWHM	Position	FWHM	Position	FWHM	Position	FWHM
Pd $3d_{5/2}$	$-0.3^\circ \pm 0.1^\circ$	9.5°	$20.7^\circ \pm 0.1^\circ$	11.2°	$35.8^\circ \pm 0.3^\circ$	8.4°	$53.9^\circ \pm 0.1^\circ$	11.7°
Pd $3d_{3/2}$	$-0.3^\circ \pm 0.1^\circ$	9.4°	$20.0^\circ \pm 0.2^\circ$	11.0°	$36.0^\circ \pm 0.1^\circ$	8.2°	$54.0^\circ \pm 0.1^\circ$	11.4°
Experiment	$-0.3^\circ \pm 0.9^\circ$		$20.4^\circ \pm 0.9^\circ$		$35.9^\circ \pm 0.9^\circ$		$54.0^\circ \pm 0.9^\circ$	
Theory	0°		19.5°		35.3°		54.7°	

TABLE II. Forward-scattering peak positions and FWHM of the Pd $3d_{5/2}$, Pd $3d_{3/2}$, and Pd $3p_{3/2}$ core-level photoelectron and Pd M_5VV Auger-electron angular distributions along the $\langle 001 \rangle$ direction, $\phi=0$. Peak positions are determined from the cubic spline fit to the data.

Transition	Position	FWHM	Position	FWHM	Position	FWHM	Position	FWHM
Pd $3d_{5/2}$	$0.2^\circ \pm 0.4^\circ$	8.1°	$19.2^\circ \pm 0.4^\circ$	11.3°	$45.2^\circ \pm 0.5^\circ$	11.3°	$70.1^\circ \pm 0.4^\circ$	7.9°
Pd $3d_{3/2}$	$0.5^\circ \pm 0.4^\circ$	7.9°	$19.5^\circ \pm 0.1^\circ$	11.0°	$45.3^\circ \pm 0.1^\circ$	11.2°	$69.9^\circ \pm 0.3^\circ$	
Pd $3p_{3/2}$	$0.4^\circ \pm 0.2^\circ$	8.2°	$19.5^\circ \pm 0.4^\circ$	11.5°	$45.7^\circ \pm 0.5^\circ$	9.7°	$70.8^\circ \pm 0.3^\circ$	8.8°
Pd M_5VV	$1.4^\circ \pm 0.3^\circ$	11.2°	$19.5^\circ \pm 0.4^\circ$		$45.6^\circ \pm 0.2^\circ$	13.0°		
Experiment	$0.6^\circ \pm 1.3^\circ$		$19.4^\circ \pm 1.3^\circ$		$45.5^\circ \pm 1.3^\circ$		$70.3^\circ \pm 1.3^\circ$	
Theory	0°		18.4°		45.0°		71.6°	

Further experiments were performed to distinguish the zeroth-order forward-focusing peaks from the first-order interference peaks in that the angular distribution of the latter would shift with kinetic energy. Zeroth-order peaks are a result of a constructive interference between the primary photoelectron wave (unscattered) and the elastically scattered electron wave which are in phase. The first-order peaks are due to the constructive interference between primary photoelectron electron waves and the component of the elastically scattered wave which are 180° out of phase.^{1,2} In Fig. 4 we present the angular distributions of the Pd $3d_{5/2}$ ($E_k=1151.5$ eV), Pd $3p_{3/2}$ ($E_k=954.5$ eV) core levels and the Pd M_5VV ($E_k=327.5$ eV) Auger transition along the $\langle 001 \rangle$ azimuth direction. First of all, we did not see a “dip” around 0° for any of the core levels and the 327.5-eV Auger electrons. The two photoelectron angular distributions were very similar to Fig. 3, with four major peaks clearly identified at polar emission angles around 0° , 20° , 46° , and 70° . The angular distribution of the 327.5-eV Auger emission preserved the first three peaks, whereas the fourth peak seems to disappear with a small shoulder around 64° . The observed anisotropies were 42% for the Pd $3p_{3/2}$ core level and 54% for the Pd M_5VV Auger transition. The FWHM values become larger with decreasing kinetic energy, as shown

in Table II. This is consistent with the notion that forward focusing is a dominant mechanism at high kinetic energies.²

We performed further experiments to investigate the response of the SCIENTA ESCA-300 using Pd polycrystalline material. The results of these experiments are shown in Fig. 5 for the same emissions as in the previous figure between $\Theta = -10^\circ$ and 74° with 2° increments. The peaks observed using single-crystal Pd were clearly not present in this case, proving that the peaks were associated with the crystallinity of the surface. According to Fig. 5, the two high-energy emissions at 1151.5 and 954.5 eV had a similar response in that both intensities dropped to $\sim 50\%$ of their initial value at $\theta = 74^\circ$. The collection of the 327.5-eV electrons was less efficient at large polar emission angles and dropped to $\sim 67\%$ of their intensity at 74° . Thus the 327.5-eV electrons were undercounted at higher emission angles with respect to the Pd $3d_{5/2}$ and Pd $3p_{3/2}$ photoelectron emissions. Tables I and II show the peak positions of the angular distributions of the photoelectron and Auger-electron emissions investigated in this study. These peak positions were determined using a cubic spline fit to the data. The error shown in the data included only the uncertainty in locating the peak position. The averaged results (now marked as “Experiment”

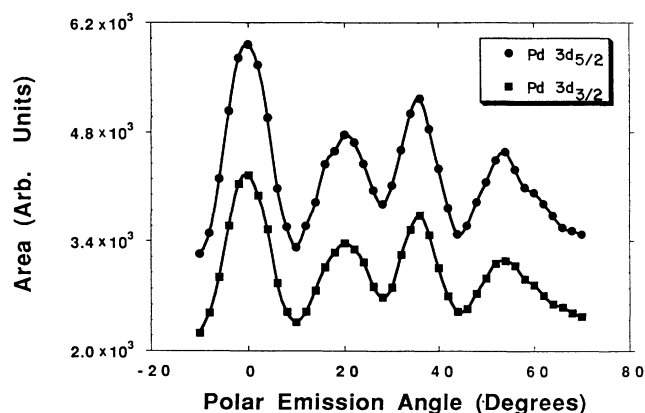


FIG. 2. Angular distributions of the Pd $3d_{5/2}$ and Pd $3d_{3/2}$ photoelectrons recorded along the $\langle 011 \rangle$ direction of Pd(100). The solid line is the cubic spline fit to the experimental data points (symbols). Major components of the peaks around 0° , 20° , 35° , and 54° were identified to be related to the forward scattering of the photoelectrons from the neighboring Pd atoms.

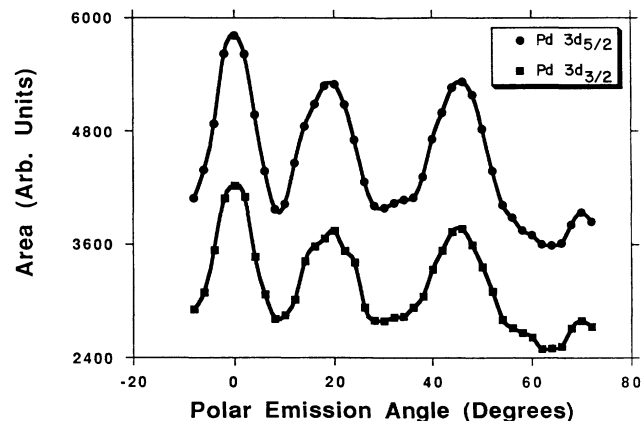


FIG. 3. Angular distributions of the Pd $3d_{5/2}$ and Pd $3d_{3/2}$ photoelectrons recorded along the $\langle 001 \rangle$ direction of Pd(100). Major components of the peaks at 0° , 20° , 46° , and 70° were identified to be related to the forward scattering of the photoelectrons from the neighboring Pd atoms.

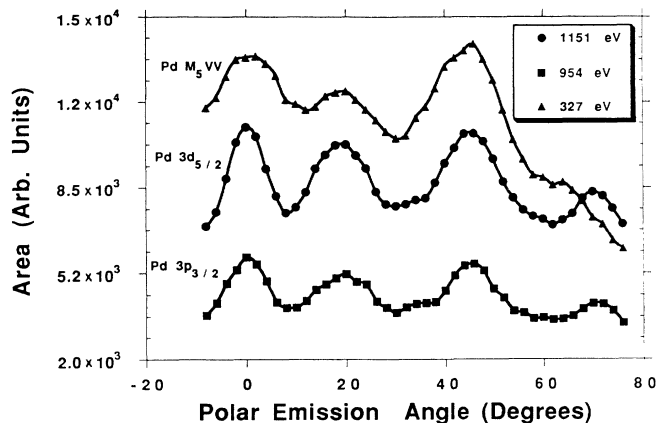


FIG. 4. Angular distributions of the Pd $3d_{5/2}$ ($E_k=1151.5$ eV) and Pd $3p_{3/2}$ ($E_k=954.5$ eV) photoelectrons and M_5VV Auger electrons ($E_k=327.5$ eV) recorded along the $\langle 001 \rangle$ direction of Pd(100). A peak around 70° seems to be missing from the Auger-electron distribution, possibly due to the sharp background shown in Fig. 5.

in Tables I and II) had the overall error of 1.3° along the $\langle 001 \rangle$ direction and 0.9° along the $\langle 011 \rangle$ direction. The measured peak positions were within $\sim 1.0^\circ$ of the expected values. Azimuthal dependence of the Pd $3d$ photoelectron distribution at a fixed polar emission angle $\theta=45^\circ$ was also investigated. The result is shown in Fig. 6. The fourfold symmetry of the Pd(100) surface was clearly observed by the two major peaks around 0° and 90° and possible first-order interference peaks in between. The experimental anisotropy was 37% for the Pd $3d_{5/2}$ and 39% for the Pd $3d_{3/2}$ core-level electron distributions. The degeneracy factor was determined to be 1.41 ± 0.05 .

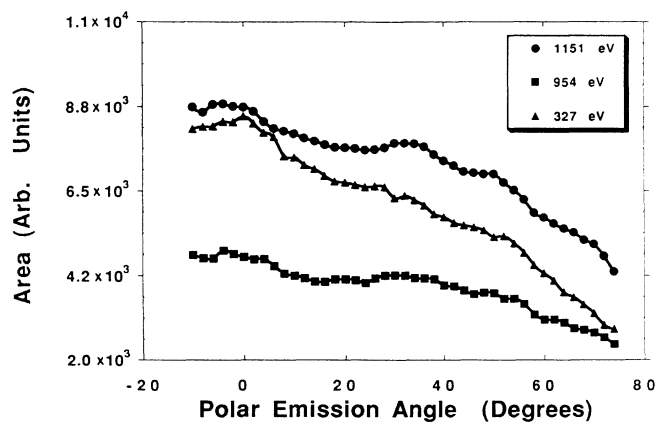


FIG. 5. Angular distributions of the Pd $3d_{5/2}$ and Pd $3p_{3/2}$ photoelectrons and M_5VV Auger electrons obtained using a polycrystalline Pd sample. An expected isotropic electron distribution was obtained. A sharp decline in the Auger-electron angular distribution at a large emission angle is observed in this case as well.

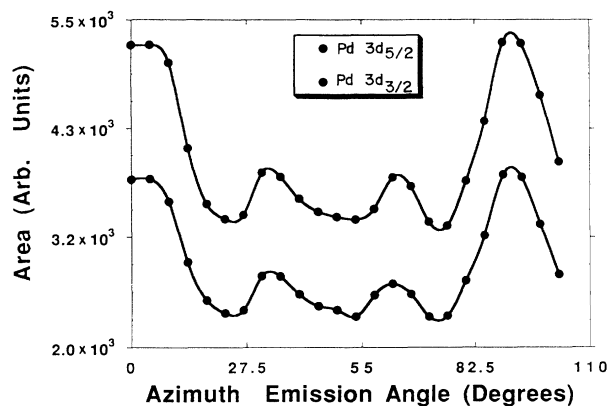


FIG. 6. Angular distributions of the Pd $3d_{5/2}$ and Pd $3d_{3/2}$ photoelectrons obtained by scanning azimuthal emission angle ϕ at a fixed polar emission angle $\theta=45^\circ$. Two major peaks observed at 0° and 90° are consistent with the fourfold nature of the Pd(100) surface.

DISCUSSION

Angular distribution of the various Pd core-level photoelectrons and Pd M_5VV Auger electrons is consistent with the forward-focusing mechanism. Angular distribution results shown in Figs. 3 and 4 can be explained with a structure shown in Fig. 7. It consists of four layers of Pd atoms along the $\langle 001 \rangle$ direction. Expected forward-focusing directions are 0° ($R=3.88$ Å), 18.4° ($R=6.13$ Å), 45° ($R=2.74$ Å), 63.4° (8.68 Å), and 71.6° ($R=6.13$ Å), where R is the emitter-scatterer distance. With the possible exception of the 63.4° peak, we have observed all of the other peaks.²² The observed angular distribution suggests that anisotropy is caused by the top four layer Pd atoms. This result is consistent with the multiple-scattering theory in that strong forward-focusing enhancements can originate from the top few atomic layers.² This is because enhancements in the forward direction cannot be sustained for larger thicknesses due to what is called “dephasing.” The deeper layers contribute to the isotropic background. A structure consistent with

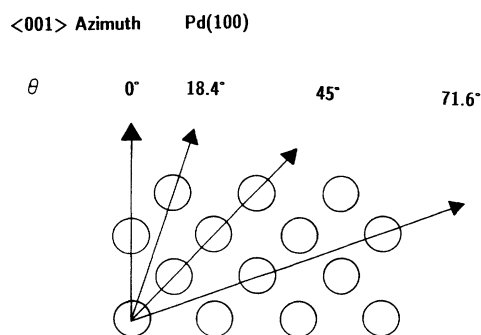


FIG. 7. Microscopic structure of the Pd(100) surface along the $\langle 001 \rangle$ direction. The observed forward-scattering angular distribution peaks are within $\sim 1.0^\circ$ of the theoretically expected values at 0° , 18.4° , 45° , and 71.6° . This suggests that the top four Pd layers contribute to the forward scattering.

the observed angular distribution along the $\langle 011 \rangle$ direction is shown in Fig. 8. Along the $\langle 011 \rangle$ direction every other layer is missing with the expected forward-focusing directions at 0° ($R = 3.88 \text{ \AA}$), 19.5° ($R = 8.23 \text{ \AA}$), 35.3° ($R = 4.75 \text{ \AA}$), and 54.7° ($R = 6.72 \text{ \AA}$). The positions of these peaks and their FWHM are listed in Table I.

In this study, a distinction between the forward-focusing peaks and the possible off-axis first-order interference peaks was made by studying the variation of the angular distribution with kinetic energy. The constancy of the first three peaks for the 327.5-eV Auger-electron distribution proves unambiguously that the major contribution to the first three peaks comes from the forward scattering of the photoelectrons and the Auger electrons by the overlaying scatterer atoms. This is because the forward-scattering peak positions are expected to be insensitive to the change in the kinetic energy, whereas the first-order off-axis interference peaks shift with energy. Change in the relative intensity of the 20° peaks at 327.5 eV with respect to the other two energies suggests that this peak may have some small contribution from the first-order interference. The sharp background around 70° makes it difficult to identify the fourth peak. This is a difficult region at which the electron collection efficiency may depend on kinetic energy in a complicated way, as suggested by the sharper decline in Auger-electron distribution in Fig. 5 in comparison with that of photoelectrons. A correction was attempted by finding a correction factor for each data point and for each kinetic energy using Fig. 5. The effect of this correction is to flatten the response shown in Fig. 4. After the correction, one gets considerable intensity around 70° for all three kinetic-energy values of the corrected data. Thus, we conclude that the majority of the 70° peak is *not* a first-order peak but it must have a significant zeroth-order forward-focusing contribution.

Another experimentally inevitable consequence is that whenever the kinetic energy is varied, the surface sensitivity of the technique also varies. This is due to the energy dependence of the electron escape depth. In the case of the Auger transition at 327.5 eV, the escaping Auger electrons come from the atoms closer to the surface,

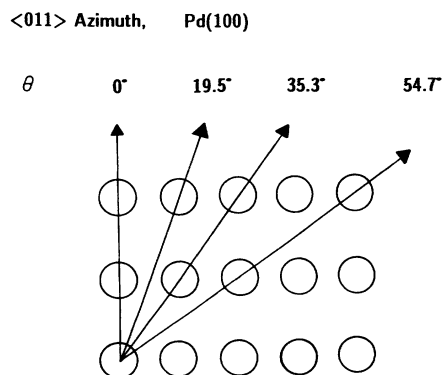


FIG. 8. Microscopic structure of the Pd(100) surface along the $\langle 011 \rangle$ direction. The observed forward-scattering angular distribution peaks are within 1.0° of the theoretically expected values at 0° , 19.5° , 35.3° , and 54.7° .

whereas the higher-energy Pd core-level photoelectrons originate from the deeper atoms. A simple explanation for the nonobservation of the 70° peak from the low-energy Auger-electron angular distribution is that, due to the increased surface sensitivity at 327.5 eV, 70° forward-focused Auger electrons cannot make it to the detector. If this is the case, we would expect the same result for the 18.4° peak which has the same emitter-scatterer distance, $R = 6.13 \text{ \AA}$, as that of the 71.6° peak. Although the 18.4° peak has a reduced intensity at low kinetic energy, it is clearly observed. Therefore, based only on its disappearance for the 327.5-eV Auger-electron distribution, it would not be prudent to assign the 70° peak as an interference peak. Also, our findings, which are based on the angular distributions using polycrystalline Pd, suggest that a decrease in the collection efficiency for the low-energy electrons at larger emission angles may be responsible for the disappearance of the 70° peak. Thus, there is no solid experimental evidence that suggests 70° is mostly an interference peak. The reductions of the intensity of the 18.4° peak at 327.5 eV suggests a small first-order contribution. It is therefore expected that the 70° peak may have a similar small first-order contribution. Also, any interference component is expected to shift only about 1° towards large angles by changing the kinetic energy of the Pd $3d_{5/2}$ and Pd $3p_{3/2}$ photoelectrons from 1151.5 to 954.5 eV. This small change would be difficult to detect in Fig. 4 accurately. We also performed single-scattering calculations based on the Poon and Tong model.⁶ We found two small peaks around 20° and 70° that are a result of the first-order constructive interference between 0° and 45° forward-focusing, and 45° and 90° forward-focusing intensities, respectively.

Auger-electron-diffraction technique has been used to measure elastic strain and relaxation at a metal-metal interface.²³ The forward-scattering spectroscopy can be used to investigate relaxations experienced by the near-surface atoms. Lateral and vertical movements of the surface atoms cause the angular distribution peaks to shift in proportion to the strength of the relaxations. These changes can be as high as 30% in the case of a body-centered-cubic (111) surface due to its open structure. From Tables I and II we conclude that our Pd(100) surface does not relax within $\sim 1.0^\circ$ ($\sim 1-2\%$). This is consistent with the LEED results for many fcc (100) surfaces due to their close structures.³ Among the other Pd surfaces, the Pd(110) face is expected to show relaxations in the order of 10%, which is likely to be detected with angle-resolved XPS.

In summary, we have experimentally shown that along the $\langle 001 \rangle$ direction 0° and 45° peaks are from the forward scattering of the next-nearest and nearest Pd atoms, respectively. The 18.4° and 71.6° peaks, although they may have a small interference component, represent the forward scattering of the photoelectrons and Auger electrons from the more-distant Pd atoms. Similarly, all of the observed angular distribution peaks along the $\langle 011 \rangle$ direction can be explained by the forward scattering of electrons by the overlying Pd atoms. These results are in agreement with the very recent results obtained with

Cu(100), Cu(110), Cu(111), Ir(111), Ni(111), and Ag(100).²⁴

ACKNOWLEDGMENTS

This work was supported by U.S. DOE Grant No. DE-FG02-86ER13580 and a grant from AMOCO cor-

poration. The authors are indebted to Dr. Alfred C. Miller for technical assistance with experiments using the SCIENTA ESCA-300 instrument and to Dr. Gary W. Simmons for providing the software for the single-scattering simulations.

-
- ¹C. S. Fadley, *Prog. Surf. Sci.* **16**, 275 (1985).
²W. F. Egelhoff, Jr., *Crit. Rev. Solid State Mater. Sci.* **16**, 213 (1990).
³F. Jona, and P. M. Marcus, in *The Structure of Surfaces II*, edited by J. F. Van der Veen and M. A. Van Hove (Springer-Verlag, New York, 1988), p. 92.
⁴H. L. Davis and T. Kaplan, *Solid State Commun.* **19**, 595 (1976).
⁵S. Kano, S. M. Goldberg, N. F. T. Hall, and C. S. Fadley, *Phys. Rev. B* **22**, 6085 (1980).
⁶H. C. Poon and S. Y. Tong, *Phys. Rev. B* **30**, 6211 (1984).
⁷E. L. Bullock and C. S. Fadley, *Phys. Rev. B* **31**, 1212 (1985).
⁸L. McDonnell, D. P. Woodruff, and B. W. Holland, *Surf. Sci.* **51**, 249 (1975).
⁹W. F. Egelhoff, Jr., *Phys. Rev. Lett.* **59**, 559 (1987).
¹⁰S. Y. Tong, H. C. Poon, and D. R. Snider, *Phys. Rev. B* **32**, 2096 (1985).
¹¹J. J. Barton, S. W. Robey, and D. A. Shirley, *Phys. Rev. B* **34**, 778 (1986).
¹²M. Sagurtan, E. L. Bullock, and C. S. Fadley, *Surf. Sci.* **182**, 287 (1987).
¹³M. L. Xu and M. Van Hove, *Surf. Sci.* **215**, (1989).
¹⁴A. P. Kaduwela, G. S. Herman, D. J. Friedman, and C. S. Fadley, *Phys. Scr.* **41**, 948 (1990).
¹⁵D. J. Friedman and C. S. Fadley, *J. Electron Spectrosc. Relat. Phenom.* **51**, 689 (1990).
¹⁶G. S. Herman, T. T. Tran, K. Higashiyama, and C. S. Fadley, *Phys. Rev. Lett.* **68**, 1204 (1992).
¹⁷B. W. Holland, L. McDonnell, and D. P. Woodruff, *Solid State Commun.* **11**, 991 (1972).
¹⁸J. R. Noonan, D. M. Zehner, and L. H. Jenkins, *J. Vac. Sci. Technol.* **13**, 183 (1976).
¹⁹D. M. Zehner, J. R. Noonan, and L. H. Jenkins, *Phys. Lett.* **62A**, 267 (1977).
²⁰L. J. Terminello and J. J. Barton, *Science* **251**, 1219 (1991).
²¹D. G. Frank, N. Batina, T. Golden, F. Lu, and A. T. Hubbard, *Science* **247**, 182 (1990).
²²Careful analysis of the 327.5-eV angular distribution yields a small shoulder around 64° before and after the correction. Since there is no sign of this peak for the other two energies, we do not claim to have seen a 63.4° forward-focusing peak.
²³S. A. Chambers, H. W. Chen, I. M. Vitomirow, S. B. Anderson, and J. H. Weaver, *Phys. Rev. B* **33**, 8810 (1986).
²⁴Z. L. Han, S. Hardcastle, G. R. Harp, H. Li, X. D. Wang, J. Zhang, and B. P. Tonner, *Surf. Sci.* **258**, 313 (1991).